

# Calculation of the bootstrap current profile for the TJ-II stellarator

J.L. Velasco<sup>1</sup>, K. Allmaier<sup>2</sup>, A. López-Fraguas<sup>1</sup>, C.D. Beidler<sup>3</sup>, H. Maassberg<sup>3</sup>, W. Kernbichler<sup>2</sup>, F. Castejón<sup>1</sup>, J.A. Jiménez<sup>1</sup>

<sup>1</sup> Laboratorio Nacional de Fusión, Asociación EURATOM-CIEMAT, Madrid, Spain

<sup>2</sup> Institut für Theoretische Physik - Computational Physics, Technische Universität Graz, Association EURATOM-ÖAW, Graz, Austria

<sup>3</sup> Max-Planck Institut für Plasmaphysik, IPP-EURATOM, Greifswald, Germany

E-mail: joseluis.velasco@ciemat.es

## Abstract.

Calculations of the bootstrap current for the TJ-II stellarator are presented. DKES and NEO-MC codes are employed; the latter has allowed, for the first time, the precise computation of the bootstrap transport coefficient in the long mean free path regime of this device. The low error bars allow a precise convolution of the monoenergetic coefficients, which is confirmed by error analysis. The radial profile of the bootstrap current is presented for the first time for the 100\_44\_64 configuration of TJ-II for three different collisionality regimes. The bootstrap coefficient is then compared to that of other configurations of TJ-II regularly operated. The results show qualitative agreement with toroidal current measurements; precise comparison with real discharges is ongoing.

## 1. Introduction

The bootstrap current is a neoclassical effect triggered by the radial gradients of the density and temperature in the presence of an inhomogeneous magnetic field, see e.g. Refs. [1, 2] and references therein.

The control of the bootstrap current, and thus of the total parallel current, may lead to the possibility of continuous operation in tokamak overdense plasmas. In stellarators, it can provide access to improved confinement regimes, by means of control of the rotational transform profile. On the other hand, the bootstrap current may perturb the desired magnetic configuration produced by the external coils. This is specially important for shearless devices, such as W7-X [3] or TJ-II [4].

Indeed, one of the main lines of research at the flexible heliac TJ-II is the relation between confinement and the magnetic configuration [5, 6, 7, 8, 9]. Ref. [10] offers a review of results at TJ-II and other stellarators. Therefore, an estimation of finite- $\beta$  effects on the characteristics of the magnetic configuration such as the rotational transform, the magnetic shear, the position of rational surfaces or the magnetic well, is of great importance. These effects are not expected to be large, since TJ-II is a heliac-type stellarator [4] consequently showing a small Shafranov shift of the magnetic surfaces, but still this should be quantified.

Additionally, an Electron Bernstein Wave (EBW) heating system is being installed at TJ-II [11]. Apart from its main purpose of heating overdense plasmas, it may be employed to drive current as well. Then, the total current (bootstrap plus the one driven by EBW) could be used to try to tailor the rotational transform profile [12, 13].

The calculation of the bootstrap current is a numerical challenge for non-axisymmetric devices, since the error estimates for computations in the long-mean-free-path (*lmfp*) regime of stellarators are usually large: DKES [14] has a convergence problem in the *lmfp* and the Monte Carlo methods have an unfavorable scaling of the computing time with the collisionality. Examples of similar calculations for non-axisymmetric devices may be found in Refs. [15, 16]. The dependence of the bootstrap current on the configuration has been explored in several devices such as W7-X [17] and Heliotron-J [18]. The former presents momentum correction techniques applied to the calculation of the bootstrap current profile for two different configurations of W7-X. In the latter, the monoenergetic bootstrap coefficient is studied as a function of the *bumpiness* of the configuration. Ref. [19] also contains a comprehensive study of the numerical results for the bootstrap coefficient, as well as the other monoenergetic transport coefficients, for several stellarators.

Despite its interest, the bootstrap current profile at TJ-II is not known with precision: the problem of lack of accuracy in the *lmfp* regime is especially relevant for this device [20, 21, 22], which is characterized by a very complex magnetic configuration. Recently, some effort has been put in calculating with precision the bootstrap coefficient, see Ref. [19] and references therein. One of the codes in Ref. [19] is NEO-MC [23], which was explicitly developed in order to overcome the problem of poor convergence in the *lmfp* regime. It combines the standard  $\delta f$  method (see Ref. [23] and references therein) with an algorithm employing constant particle weights and re-discretizations of the test particle distribution. Apart from the monoenergetic bootstrap coefficient, NEO-MC also calculates the radial diffusion coefficient, required for calculating the ambipolar electric field, and the parallel conductivity coefficient, required for the momentum correction techniques [17, 24].

In this work, we show that NEO-MC is able to provide, for the first time, calculations of the contribution of the *lmfp* regime to the bootstrap current of TJ-II with high accuracy. We present, for the 100\_44\_64 magnetic configuration of TJ-II, computations of NEO-MC of the monoenergetic bootstrap coefficient at several radial positions for a wide range of collisionalities and radial electric fields. This allows, by means of energy convolution and momentum correction technique, to estimate the profile of the bootstrap current. A Monte-Carlo technique for calculating error propagation allows us to state quantitatively that the results shown are of significance.

TJ-II is a flexible Heliac whose magnetic configuration can be modified, both on a shot-to-shot basis [5, 6, 7, 8] or continuously [9]. The bootstrap current may change, even qualitatively, for different magnetic configurations of TJ-II [21]. We have thus explored part of the set of magnetic configurations of TJ-II with DKES calculations.

This work is organized as follows. In Section 2, we describe the calculation of the bootstrap current: we present the equations, we outline the difficulties that may arise when solving them and we briefly describe the algorithm employed. Then, we particularize the discussion to the TJ-II stellarator: in Section 3, we show the results. We first discuss the monoenergetic calculations, then the profile of the current

and finally the scan in magnetic configurations. Section 4 is devoted to the conclusions.

## 2. Basic theory and calculation method

In order to estimate the bootstrap current, one has to solve the Drift Kinetic Equation (DKE) that describes the evolution of the particle distribution function [14]:

$$\left( \frac{\partial}{\partial t} + \mathbf{v}_g \cdot \nabla - \mathcal{L}_c \right) \hat{f} = \mathbf{v}_g \cdot \nabla \psi, \quad (1)$$

where  $\mathbf{v}_g$  is the guiding center drift velocity,  $\psi$  is the toroidal magnetic flux through the local magnetic surface and  $\mathcal{L}_c$  is the collision operator. Here  $\hat{f}$  is the normalized perturbation of the distribution function  $f$  and it is defined through the local Maxwellian distribution function  $f_M$ :

$$f = f_M - \hat{f} \frac{\partial f_M}{\partial \psi}. \quad (2)$$

The neoclassical ordering [2] allows to neglect the time-dependence of  $\hat{f}$ , as well as its radial variation. The equations become *local*, i.e., the radial position enters only as a parameter. If the  $\vec{E} \times \vec{B}$  drift included in  $\vec{v}_g$  is treated as incompressible [25], the neglect of energy diffusion in the Lorentz collision operator allows for monoenergetic solution of the equations: the kinetic energy can also be considered a parameter. The remaining equation is then three-dimensional.

Ignoring momentum-correction for the moment, the fluxes may be expressed as linear combinations of the gradients of density and temperature and of the electric field. The following expressions, together with their derivation, may be found for instance in Ref. [19]. For each species  $b$ , the radial particle flux and the bootstrap current are:

$$\frac{\langle \Gamma_b \rangle}{n_b} = -L_{11}^b \left( \frac{1}{n} \frac{dn}{dr} - Z_b e \frac{E_r}{T_b} - \frac{3}{2} \frac{1}{T_b} \frac{dT_b}{dr} \right) - L_{12}^b \frac{1}{T_b} \frac{dT_b}{dr}, \quad (3)$$

$$\frac{\langle \vec{j}_b \cdot \vec{B} \rangle}{Z_b e n B_0} = -L_{31}^b \left( \frac{1}{n} \frac{dn}{dr} - Z_b e \frac{E_r}{T_b} - \frac{3}{2} \frac{1}{T_b} \frac{dT_b}{dr} \right) - L_{32}^b \frac{1}{T_b} \frac{dT_b}{dr}. \quad (4)$$

As usual,  $Z_b$ ,  $T_b$  and  $n$  are the charge number, temperature and density of species  $b$ ;  $e$  is the elemental charge and  $E_r$  is the radial electric field;  $b = e$  are electrons and  $b = i$  are protons.  $B_0$  is the (0,0) Fourier harmonic of the field in Boozer coordinates and the brackets denote flux-surface average. The thermal coefficients  $L_{ij}$  at each radial position are calculated by convolution with a Maxwellian distribution of the monoenergetic coefficients:

$$L_{ij}^b(r, n, T_i, T_e, E_r) = \frac{2}{\sqrt{\pi}} \int_0^\infty dx^2 e^{-x^2} x^{1+2(\delta_{i,2}+\delta_{i,2})} D_{ij}(r, \nu^*, \Omega), \quad (5)$$

where  $x = v/v_{th}^b$  is the particle velocity normalized by the thermal velocity of species  $b$ ;  $\delta_{i,2}$  is the Kronecker delta. The monoenergetic coefficients  $D_{ij}$  depend on the radially local magnetic field strength, and are calculated and stored in a database for fixed values of the collisionality  $\nu^* = \nu R/\nu_i$  and the *electric field parameter*  $\Omega \equiv E_r/(vB_0)$ . Here,  $\nu$  is the collision frequency (see Ref. [19] for its explicit form),  $R$  the major radius of the device and  $\iota$  the rotational transform. There is one independent simulation for each value of  $r$ ,  $\nu^*$  and  $\Omega$ , from which we obtain the three independent monoenergetic transport coefficients  $D_{11}$ ,  $D_{31}$  and  $D_{33}$  (note that  $D_{11} = D_{12} = D_{21} = D_{22}$  and

$$D_{31} = D_{32} = D_{13} = D_{23}.$$

Following Eqs. (4) and (5), one needs to compute and convolute the monoenergetic bootstrap coefficient  $D_{31}$  in order to calculate the thermal coefficients  $L_{31}^b$  and  $L_{32}^b$  which relate the parallel current to the thermodynamic forces. This convolution must be done for a given radial electric field  $E_r$ , that is obtained from the ambipolar condition  $\langle \Gamma_e \rangle(E_r) = \langle \Gamma_i \rangle(E_r)$ . Thus, according to Eq. (3), the radial diffusion coefficient  $D_{11}$  must also be computed in order to estimate  $L_{11}^b$  and  $L_{12}^b$ , which relate the radial particle fluxes to the thermodynamic forces.

Finally, the Lorentz collision operator does not conserve momentum. For this reason, momentum-correction techniques are included in the calculation, following method 2 in Ref. [17]. Then, the linear relation of Eqs. (3) and (4) is not correct anymore (but still allows the discussion of the qualitative behaviour of the bootstrap current in terms of the transport coefficients and the plasma gradients). For these techniques, one needs also to calculate the parallel conductivity coefficient  $D_{33}$ .

One must note that the local ansatz underlying this approach is only partially fulfilled at certain positions of TJ-II [26, 27]. This makes the diffusive picture of transport only approximately valid. Nevertheless, relaxation of the local ansatz would make the calculation of the bootstrap current profile impossible in terms of computing time. Also the monoenergetic picture [28] breaks down for very large electric fields.

### 2.1. The $\delta f$ method

Solution of Eq. (1) in order to calculate the bootstrap current is a numerical challenge. The reason is that one has to calculate an asymmetry in the particle distribution function caused by a combination of plasma radial gradients and particle trapping between local maxima of the magnetic field strength. Although the trapped particles do not provide a large current, the passing particle population equilibrate with them via collisions. Then, when it comes the time to calculate this effect by estimating  $D_{ij}$  by means of a Monte-Carlo code, one has to be able to estimate the non-compensation of the current carried by co-passing particles and that carried by counter-passing particles. Note that the trapped-particle fraction is a radially local quantity determined by the variation of the magnetic field strength in the local flux-surface labelled by  $r$ . Therefore, the dependence of the transport coefficients (and specifically of the bootstrap coefficient) on the trapped-particle fraction is implicitly accounted for in  $D_{ij}(r, \nu^*, \Omega)$  of Eq.(5).

Additionally, in stellarators, particle trapping may be toroidal or helical [1], and these two components may add one to the other or cancel depending on the magnetic configuration.

Finally, in  $\delta f$  Monte Carlo methods, the contribution of each test particle to the monoenergetic coefficient is proportional to its radial excursion from the original magnetic surface. Therefore, the contribution of the trapped particles consists of relatively large terms which numerically cancel out. This is the issue that is addressed with NEO-MC.

NEO-MC [23] is an improved  $\delta f$  Monte Carlo method developed for computation of mono-energetic neoclassical transport coefficients in stellarators. This method uses a re-discretization procedure and importance sampling in order to reduce the variance of these coefficients. As a result, the CPU time required for a given accuracy of the

computation of the bootstrap coefficient scales as the mean free path to the power of  $3/2$ . This method introduces no bias from filtering out particles. In addition, it allows simultaneous computation of the bootstrap coefficient and the diffusion coefficient. NEO-MC has been benchmarked with other Monte Carlo and field-line-tracing methods and with DKES, for different magnetic configurations and for a range of values of the collisionality and the electric field [19]. The results are in good agreement, and we make use of both NEO-MC and DKES in the following.

## 2.2. Error estimate

Although NEO-MC (and DKES for not too low collisionalities) provide small error bars, the total current may be close to zero: since the helical and the toroidal contributions, as in every classical stellarator, have opposite signs, they may exactly cancel out at a given collisionality. Therefore some error estimate is required in order to assess if the uncertainty in  $D_{ij}$  renders the calculated currents inaccurate. In this section, we show a method for doing so.

Although Eq. (1) is linear,  $v_g$  includes the radial electric field, which we calculate by means of the ambipolar condition by root-finding (we select among multiple roots according to a thermodynamic condition, see e.g. [29]). Therefore  $L_{ij}(E_r)$  are employed to calculate  $E_r$  itself. In this non-linear calculation, error propagation from the monoenergetic coefficients to the bootstrap current profile may become cumbersome.

We therefore undertake a Monte Carlo error propagation. We start from a database of monoenergetic transport coefficients with their corresponding error bars, which we have previously calculated with NEO-MC or DKES. We then take a *sample* of the database: at every radial position  $\rho$ , for every value of  $\nu^*$ , and  $\Omega$ , we give numerical values to  $D_{11}$ ,  $D_{31}$  and  $D_{33}$ . We do so by generating, at every point in the  $(\rho, \nu^*, \Omega)$ -space, three independent Gaussian random numbers according to the average values and error bars of the coefficients stored at the database. Then, convolution, momentum-conserving and root-finding techniques provide the ambipolar electric field and the neoclassical fluxes for this particular *realization* of the neoclassical database. Averaging over 50 of such samples is usually enough to present the bootstrap current profile with a meaningful variance. Here,  $\rho = \sqrt{\psi/\psi_0} \equiv r/a$  is the normalized radial coordinate, where  $\psi_0$  is the toroidal flux through the last closed magnetic surface.

This procedure may also be straightforwardly extended to account for the uncertainty in plasma profiles, although, as we show below, we do not consider error bars in our density and temperatures in this work.

## 3. Calculation and results

### 3.1. Magnetic configuration

TJ-II is a medium size  $N = 4$  heliac with bean-shaped plasma cross-section and strong helical variation of its magnetic axis. The magnetic configuration employed for these calculations is the so-called 100\_44\_64, the most often employed during the experimental campaign of TJ-II. The major radius of this configuration is  $R = 1.504$  m, the minor radius is  $a = 0.192$  m and the volume-averaged magnetic field is 0.957 T. The iota profile is fairly flat, with  $\iota(0) = -1.551$  and  $\iota(a) = -1.650$ . The vacuum equilibrium

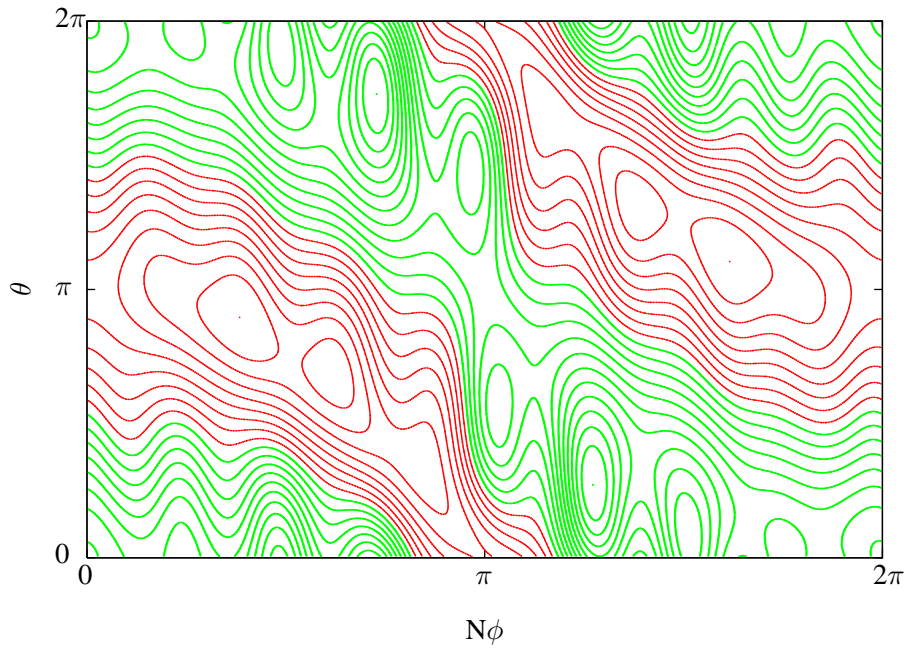


**Figure 1.** Contour plot of  $B$  at  $\rho = 0.5$ . Red (black) corresponds to  $B/B_0 > 1$  and green (grey) corresponds to  $B/B_0 < 1$ . Two consecutive lines differ by 0.015.

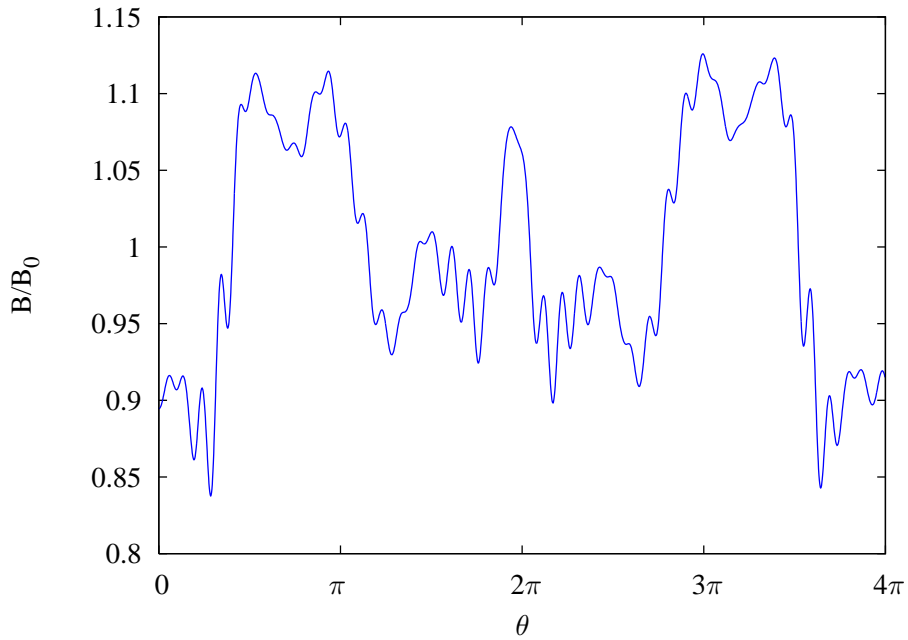


**Figure 2.** Variation of  $B/B_0$  along the magnetic field line passing through  $\theta = 0$  at  $\rho = 0.5$ .

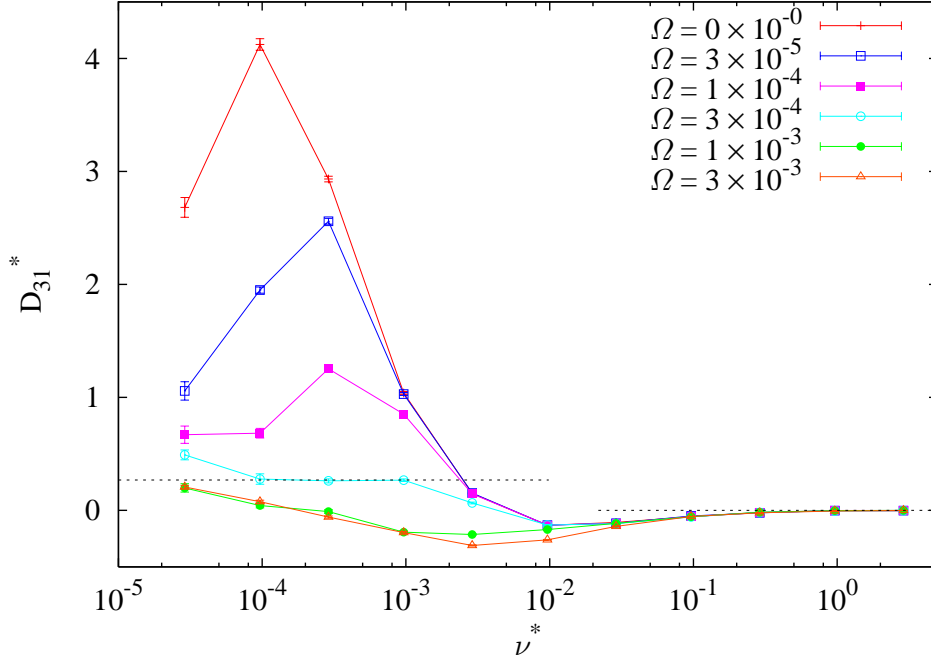


**Figure 3.** Monoenergetic bootstrap coefficient at  $\rho = 0.5$  as a function of the collisionality for different electric fields. The dashed lines represent the  $\nu^* \rightarrow 0$  and  $\nu^* \rightarrow \infty$  limits.

is used here. In Fig. 1 we plot the contours of constant magnetic field strength  $B$  at the flux-surface given by  $\rho=0.5$ , where  $\theta$  and  $\phi$  are the poloidal and toroidal angles in Boozer coordinates. The structure of deep localized minima and maxima is apparent. Fig. 2 show the variation of  $B$  along a field line starting at  $\theta=0$   $\phi=0$ , which clearly cannot be described with a few Fourier modes. Hence the convergence problems of DKES.

### 3.2. Monoenergetic coefficients

We have calculated, for the configuration described in the previous subsection, the monoenergetic coefficient  $D_{31}$ , together with  $D_{11}$  and  $D_{33}$  for a wide range of the collisionality and the electric field parameter. We calculate the dependence of the monoenergetic coefficient with  $\nu^*$  (between  $3 \times 10^{-5}$  and  $3 \times 10^2$ ) for fixed values of  $\Omega$  between 0 and  $1 \times 10^{-1}$ . We have repeated these calculations at several radial locations, from  $\rho=0.08$  to  $\rho=0.98$ .

Part of the results, at middle radial position ( $\rho=0.5$ ) are shown in Fig. 3. The monoenergetic coefficient is presented there normalized to that of an axisymmetric tokamak of the same aspect ratio in the banana regime:

$$D_{31}^* \equiv D_{31}/D_{31}^b, \quad D_{31}^b = 1.46 \frac{m_b v^2}{3B_0 \nu \sqrt{\varepsilon} Z_b e}, \quad (6)$$

where  $\varepsilon$  is the inverse aspect ratio and  $m_b$  the particle mass. The results for  $D_{31}^*$

are qualitatively similar to those observed for LHD, CHS, W7-AS and others [19]: for  $\nu^* > 1$ , the collision frequency  $\nu$  is larger than the bounce frequency, hence there are no trapped particles and no seeding mechanism for the bootstrap current. Note that the monoenergetic coefficient is already close to zero for lower collisionalities than  $\nu^* = 1$ , for the bounce frequency is smaller than the *effective-detraping collision frequency*, which may be defined as  $\nu/\varepsilon$ . For very low collisionalities, as the ratio between the electric field  $\Omega$  and the collisionality  $\nu^*$  increases, the coefficient converges to an asymptotic value depending on the configuration and the radial position [30, 31]. The predicted asymptotic limit has been calculated by means of field-line integration [32].

Low error bars are obtained in the whole range of collisionalities calculated while, for this configuration, DKES cannot provide accurate values for collisionalities lower than  $3 \times 10^{-4}$ . Actually, these small error bars push the convergence with collisionless asymptote towards collisionalities even lower than  $3 \times 10^{-5}$ . In the case of very small (especially zero) electric field parameter, this seems to happen at collisionalities that are completely out of reach for our computing resources. Nevertheless, for the collisionalities of the plasmas presented in Section 3.3, the data of Fig. 3 allow for a precise calculation of the bootstrap current. Only under reactor conditions ( $n \sim 3 \times 10^{20} m^{-3}$ ,  $T \sim 20$  keV) would  $\nu^* \sim 5 \times 10^{-5} - 10^{-4}$  correspond to thermal particles.

Additionally, for some values of  $\Omega$  such as  $3 \times 10^{-4}$ , the monoenergetic coefficients do not converge to the collisionless limit. This effect was already been observed in Ref. [19], and is still to be understood. Nevertheless, one has to keep in mind that for large values of the electric field, the starting hypothesis of the calculation are not fulfilled anymore [25, 27]: the kinetic energy is not an approximately conserved quantity. Fortunately, the electric field in this region of TJ-II is low enough, specially for NBI plasmas, and these data will not be required.

Special attention must be paid to the interpolation and extrapolation of the monoenergetic database and to the calculation of the integral in Eq. (5). This integration is made by means of Gauss-Laguerre of order 64, and interpolation by 3-point Lagrange, with  $\nu^*$  and  $\Omega$  in logarithmic scale. In extrapolation, as in Ref. [33], we have made use of the asymptotic limit where available, but also tried extrapolations such as  $D_{31}^*(\nu^* < 3 \times 10^{-5}) = D_{31}^*(\nu^* = 3 \times 10^{-5})$ . We have made sure that none of these choices affects the final result.

Once we have fully covered the relevant range of collisionalities with enough accuracy, the next step in the calculation of the bootstrap coefficient is to convolute the results shown in Section 3.2 with a Maxwellian distribution function. Then, the solution of a linear system of moment equations for which the coefficients are different energy moments of the mono-energetic transport coefficients [17] allows for the calculation of the ambipolar electric field and then the bootstrap current.

### 3.3. Current profile

The bootstrap current has been estimated to be of the order of 1 kA for low density plasmas of TJ-II [22, 34]. Since the magnetic field of TJ-II has a very broad Fourier spectrum, calculation in the *lmfp* regime is very complicated, and the results presented large error bars for low collisionalities [20, 21, 22]. It has been argued that, due to the exponential in Eq. (5), the unacceptably large error bars for  $\nu^* \sim 10^{-4}$ , well into

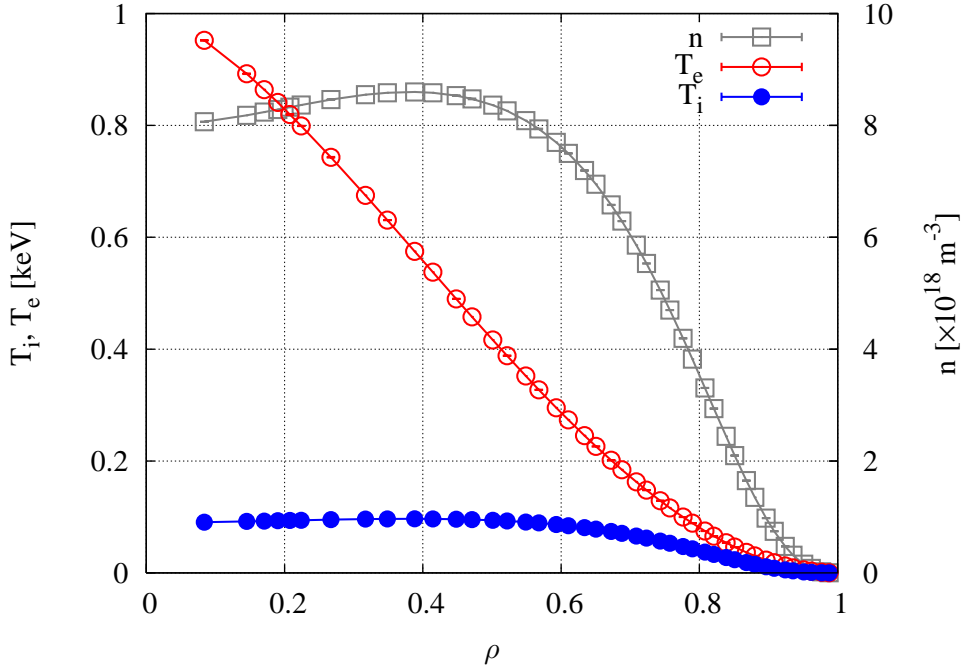


**Figure 4.** Plasma profiles for a low-density plasma of TJ-II.

the *lmfp* might not preclude the calculation of the bootstrap current [22], but this was not quantified as we propose in Section 2.2. These neoclassical calculations were compared to the measurements of the toroidal rotation velocity of some protons and impurities by means of passive emission spectroscopy [35]. Although there was some qualitative agreement, the results differed by a factor 2.

Recently, lithium wall coating at TJ-II [36] has given access to low impurity concentration and high density at plasmas heated with Neutral Beam Injection. For these plasmas, in which the *lmfp* regime is less relevant, the bootstrap current should be easier to calculate. Nevertheless, being smaller in magnitude, the significance of the results must be checked.

We calculate the bootstrap current profile for three regimes of TJ-II, corresponding to low, medium and high density. Figs. 4, 5 and 6 show plasma profiles characteristic of the three regimes. Low density plasmas at TJ-II have peaked electron temperature profiles, with central values of above 1 keV and hollow density profiles. As the density rises, both profiles become flatter and the electron temperature becomes lower, of about 200 —300 eV for high density plasmas heated by means of Neutral Beam Injection. The ion temperature is rather flat under all conditions, of the order of 100 eV. For these plasmas with lithium-coated walls, taking the effective charge  $Z_{eff}=1$  is a reasonable approximation. Note that, since for thermal particles  $\nu^* \propto n/T^2$ , higher density means higher collisionality, for the temperature decreases (for electrons) or barely changes (for ions).

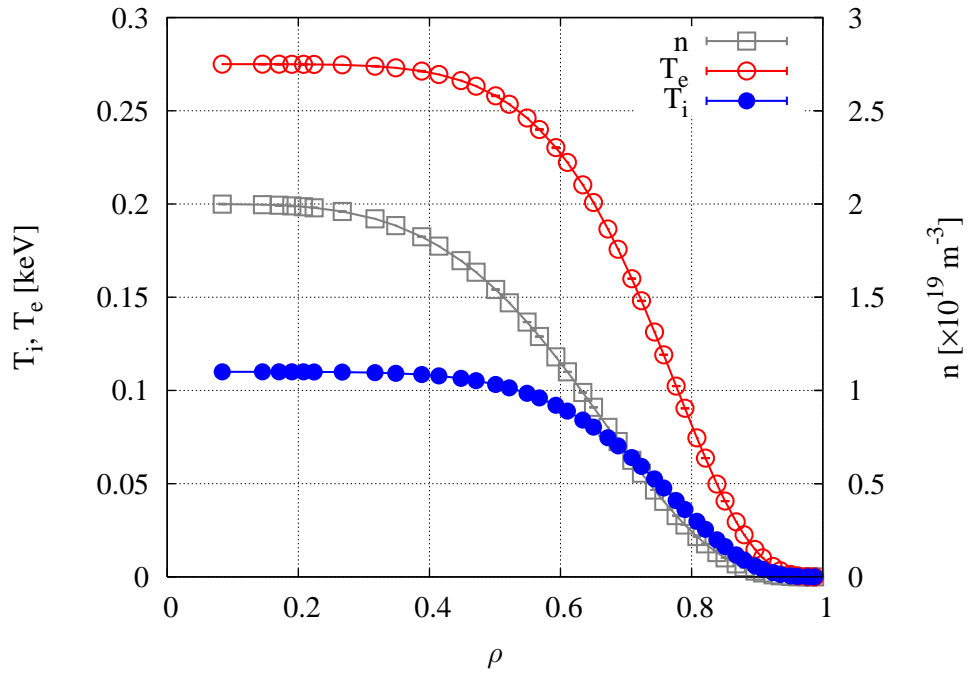


Figure 5. Plasma profiles for a medium-density plasma of TJ-II.

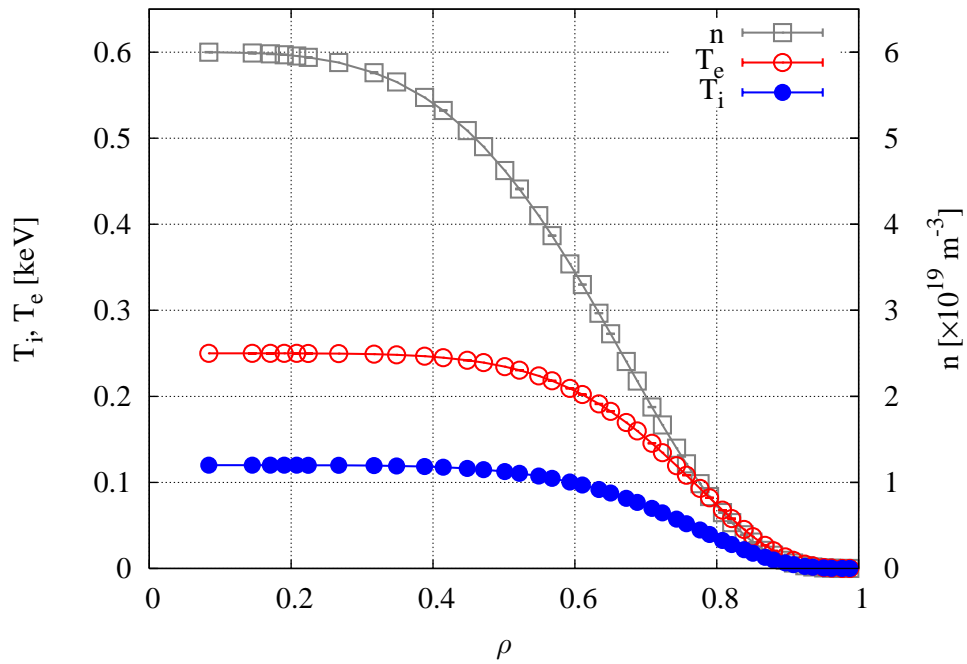
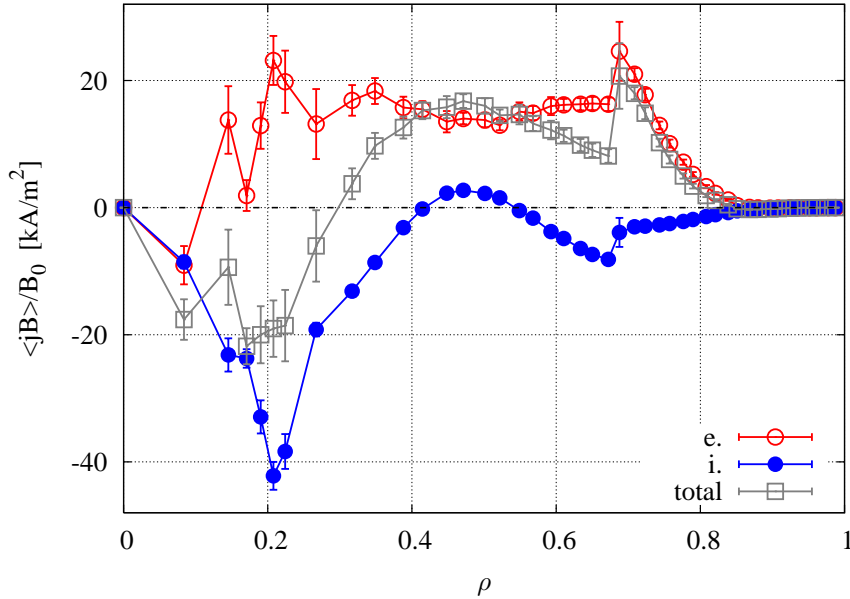


Figure 6. Plasma profiles for a high-density plasma of TJ-II.



**Figure 7.** Calculated bootstrap current profile for the low density plasma. The error bars are calculated following Section 2.2

We show the results in Figs. 7, 8 and 9, separating the contributions from electrons and ions. The latter may be compared to toroidal rotation measurements at TJ-II [35], available for low density plasmas.

Some general features may be extracted from observation of the three figures. First of all, the current is mainly carried by the electrons. This is a consequence of the decoupling of the ion and electron temperatures, the latter being systematically higher, in TJ-II plasmas. Thus, the electrons are much less collisional and their contribution is much higher. Also, for the high-density cases (and the low density at outer positions), the plasma is in the *ion root* [37]: a negative radial electric field partially cancels out the ion channel while adding an additional contribution to the electron channel, see Eqs. (3) and (4). The exception are the inner radial positions in the low-density case, where the electron root is realized. There, the positive radial electric field drives a relatively high ion parallel flow (with low damping from the small trapped-particle friction) and the electron flow is coupled to it [17]. Also near the gradient zone of high density plasmas the temperatures are similar and the ion bootstrap current is not negligible.

The maxima of the bootstrap current density follow those of the temperature gradient, since  $L_{32}^e - 1.5 L_{31}^e$  is systematically much higher than  $L_{31}^e$ . This reflects the *overshoot* in the bootstrap coefficient for collisionalities between  $10^{-4}$  and  $10^{-3}$ , a usual feature in stellarators [19]. The higher the electron collisionality, the lower the amplitude of the maxima.

There is a switch in the sign of the bootstrap current at medium radius, corresponding to a switch in the sign of the electron contribution. It may be traced-back as the change of sign in the bootstrap coefficient, corresponding to the cancellation of the stellarator-like and the tokamak-like contributions. This

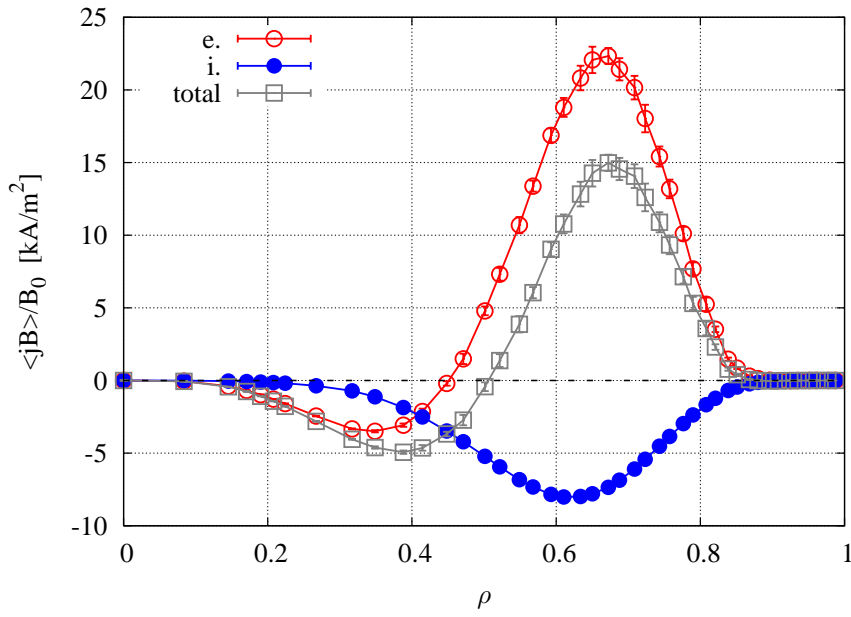


Figure 8. Calculated bootstrap current profile for the medium density plasma.

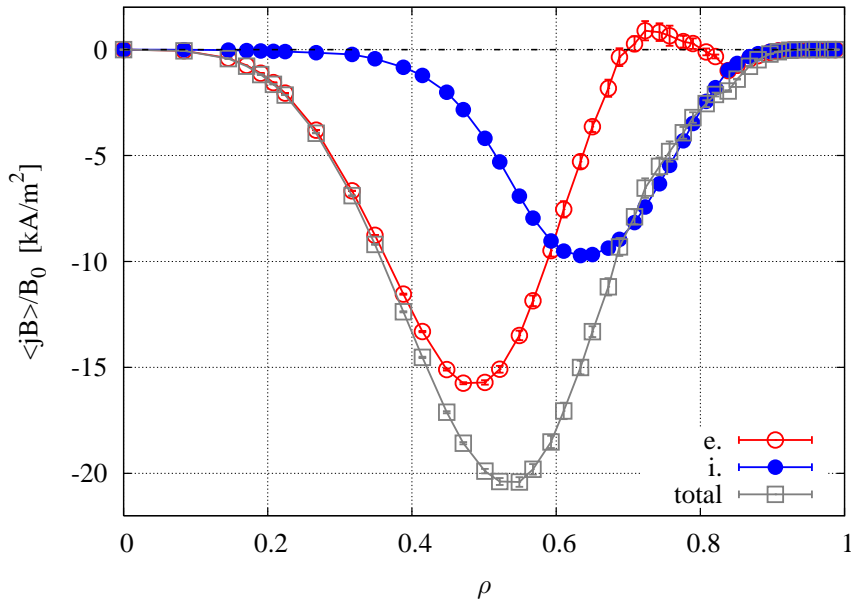


Figure 9. Calculated bootstrap current profile for the high density plasma.

happens for a given collisionality at each radial position (at medium radius, around  $\nu^* = 3 \times 10^{-3}$ , see Fig. 3). For higher densities, the switch in sign happens for larger minor radius. The consequence of this fact is that the total toroidal current is positive (tokamak-like) for low density plasmas and becomes negative (stellarator-like) for high densities. Integration of Figs. 7, 8 and 9 yield the following total currents, with the error bars in parentheses: 0.55(2) kA for the ECH plasma, 0.314(8) kA for the medium density NBI plasma and  $-0.739(3)$  kA for the high density plasma. This change of sign in the toroidal current has been observed in TJ-II operation, and the values obtained here are comparable to that measured by Rogowski coils [34].

The current in Fig. 7 presents a discontinuous behaviour around  $\rho = 0.69$ . It corresponds to the transition from electron to ion root: two stable roots exist from  $\rho=0.63$  to  $\rho=0.71$  and the electric field is evaluated by root-finding, so the transition layer is very narrow. If a differential equation for the electric field [29] were solved instead, the transition layer would be broader and Fig. 7 would become smoother. The qualitative results would be the same, with a total toroidal current ranging between 0.5 and 0.75 kA. These results remain also of significance if error bars of 20% are allowed in the density and temperature profiles.

A consequence of the high collisionality of the ions is that their contribution to the bootstrap current suffers from very low error bars, while those of the electron contribution are much higher. Therefore, comparison of these results with measurements by Charge-Exchange recombination spectroscopy (CXRS) is to be done. Actually, much of the error bars in Figs. 7, 8, 9 comes from the uncertainty in  $D_{33}$  coefficient for low collisionality, which is calculated with DKES and employed in the momentum-correction techniques. Although still the results are of significance, the calculation of  $D_{33}$  with NEO-MC is underway.

In Fig. 10 we show an estimate of how the bootstrap current modifies the rotational transform profile. We also plot the rationals present in the plasma for the 100\_44\_64 configuration. In the vacuum iota range, calculated with VMEC [38], several rationals (14/9, 11/7, 8/5 and 13/8) are present. Since the total toroidal current is small in absolute value for TJ-II, the most external rational barely moves. Inner rationals do move for ECH plasmas, which have plasma gradients for small minor radius. Note that negative currents lead to reduced  $|\iota|$ , and hence unwind the rotational transform.

The calculation presented is a linear approximation to a non-linear problem: this current is, as stated before, the result of the combination of the non-uniformity of the magnetic field in the flux surfaces and the density and temperature profiles. Since the calculated current is not zero, it will modify the vacuum magnetic field. The calculation of the bootstrap current should be iterated in the new magnetic configuration, and the process should be repeated until one achieves convergence (i.e., the calculated current does not vary from one iteration to the next). This type of calculation has been made for LHD [39], which is a high- $\beta$  device with relatively large bootstrap current and large Shafranov shift. It has also been performed for simplified models of NCSX and QHS [40], in order to study the preservation of the quasi-symmetry. Since TJ-II lacks any of these quasi-symmetries, is designed to have small Shafranov shift, and the pressures and calculated currents are low, it is not necessary to iterate further.

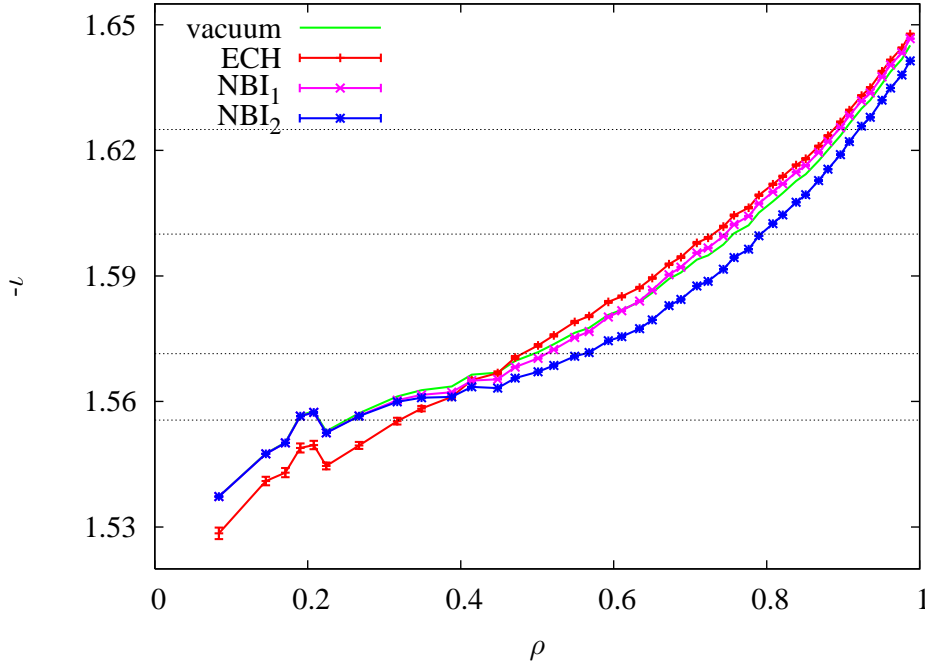


**Figure 10.** Rotational transform profile corresponding to the vacuum configuration and the three plasma profiles.

Configuration name	$\langle B(T) \rangle_{vol}$	$V(m^3)$	$\iota(0)$	$\iota(a)$
100_32_60	1.087	0.934	-1.423	-1.517
100_38_62	0.971	1.031	-1.492	-1.593
100_40_63	0.960	1.043	-1.510	-1.609
100_42_63	0.931	1.079	-1.534	-1.630
100_44_64	0.962	1.098	-1.551	-1.650
100_46_65	0.903	1.092	-1.575	-1.676
100_50_65	0.962	1.082	-1.614	-1.704
100_55_67	0.964	1.073	-1.659	-1.739

**Table 1.** Main parameters of the configuration scan

### 3.4. Configuration dependence of the bootstrap current

Finally, we make a scan in a relevant part the configuration space of TJ-II. A thorough study of the dependence of the parallel fluxes on the magnetic configuration is beyond the scope of this work; and also NEO-MC computations, although feasible, are quite time consuming. We thus try to describe the bootstrap current of the configuration in terms of its monoenergetic coefficient at  $\rho = 0.25$  and  $\rho = 0.7$  (where the electron temperature gradients are larger for low and high density plasmas respectively) for  $\Omega = 0$ . We calculate so for seven different configurations which are regularly explored in TJ-II operation. We show in Table. 1 the main global parameters: when switching

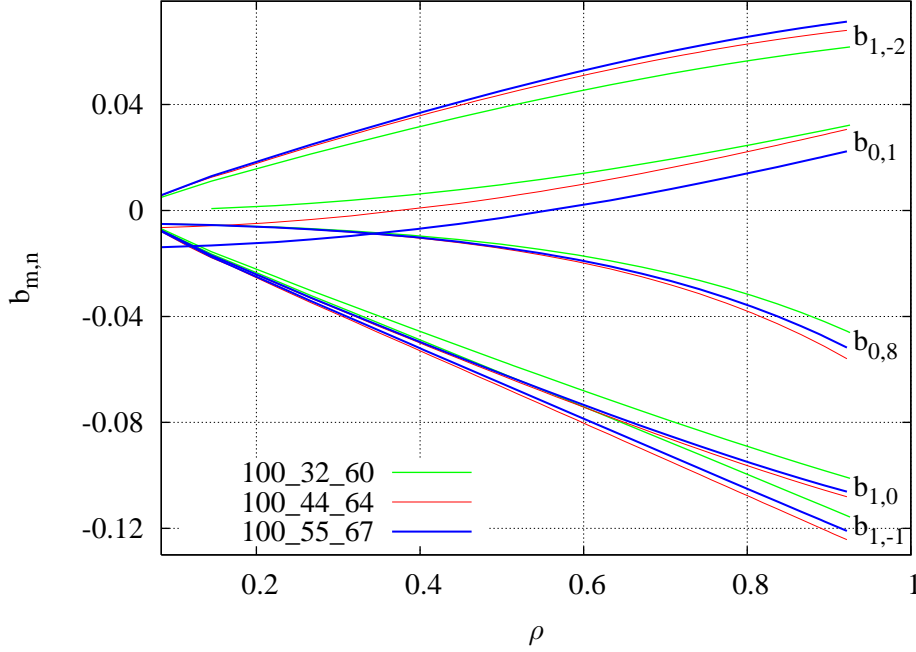


**Figure 11.** Main Fourier harmonics of the configurations 100\_32\_60, 100\_44\_64, 100\_55\_67

from one configuration to another, the volume is held approximately constant, while the rotational transform profile is raised without changing the shear. The neoclassical transport of these configurations is not expected to change much, since the main Fourier terms in the description of the magnetic field remain unchanged: Fig. 11 shows the radial profile of the main terms in the Fourier decomposition in Boozer coordinates (see Ref. [41] for a more comprehensive discussion), given by

$$B(\rho, \phi, \theta)/B_0(\rho) = \sum_{n=-\infty}^{\infty} \sum_{m=0}^{\infty} b_{m,n}(\rho) \cos(m\theta - Nn\phi). \quad (7)$$

For the sake of clarity, only the standard 100\_44\_64 configuration and the extremes of the scan (100\_32\_60 and 100\_55\_67), are presented in the plot. The two main Fourier components relevant for the bootstrap coefficient are the helical curvature  $b_{1,-1}$  and the toroidal curvature  $b_{1,0}$ . These components vary a few percents during the configuration scan. The next contribution may come from the toroidal mirror  $b_{0,1}$  [15, 18]. This is the component of largest relative variation during the magnetic scan, even reversing its sign. Nevertheless,  $b_{0,1}$  is small compared with the two curvatures and therefore it does not have a large absolute impact on the bootstrap current, as we will see below. The relative variation in the remaining components of the Fourier spectrum is negligible.

The calculation is made with DKES: up to 150 Legendre polynomials and up to 2548 Fourier modes have been employed in the description of the distribution function and the largest 50 Fourier modes have been kept in the description of the magnetic field on every surface. We have made sure that increasing the number of modes does

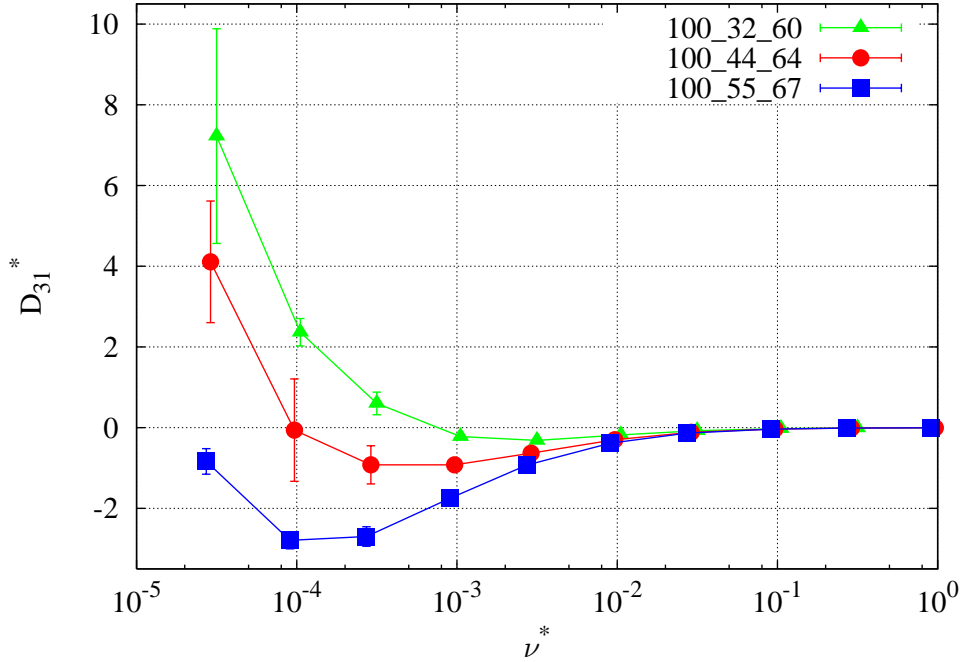


**Figure 12.** Bootstrap current coefficient at  $\rho = 0.25$  as a function of the collisionality

not modify the presented results within the error bars.

In Figs. 12 and 13 we show the collisionality dependence of the bootstrap coefficient for three different configurations at  $\rho=0.25$  and  $\rho=0.7$ . For the sake of clarity, only configurations 100\_32\_60, 100\_44\_64 and 100\_55\_67 will be shown in the figures. Since the  $D_{31}^*$  coefficient has already been discussed, we focus on the differences between configurations. Although the calculations suffer from large error bars for low collisionalities, one may see that the normalized coefficients coincide for large collisionality and differ only for small collisionalities. The differences are relatively (but not absolutely) larger for small minor radius. At this region, the toroidal and helical curvatures are relatively smaller, and therefore differences in the toroidal mirror trapping show up in the bootstrap coefficient.

A  $1/\nu$  dependence of the bootstrap current is thus to be expected (since  $D_{31} \propto D_{31}^* / \nu$ ) for the medium and high-density plasmas of Figs. 5 and 6.

For low-density plasmas, the situation is different for three reasons: first of all, the electron collisionality is significantly lower. Also the electron temperature gradient is large, see Fig. 4, so the contribution of the term proportional to  $L_{32}^e$  in Eq. (4) becomes larger. Finally, this gradient is large also for inner positions, where the differences in  $D_{31}^*$  are relatively larger, see Fig. 12. The three facts tend to maximize the difference between configurations.

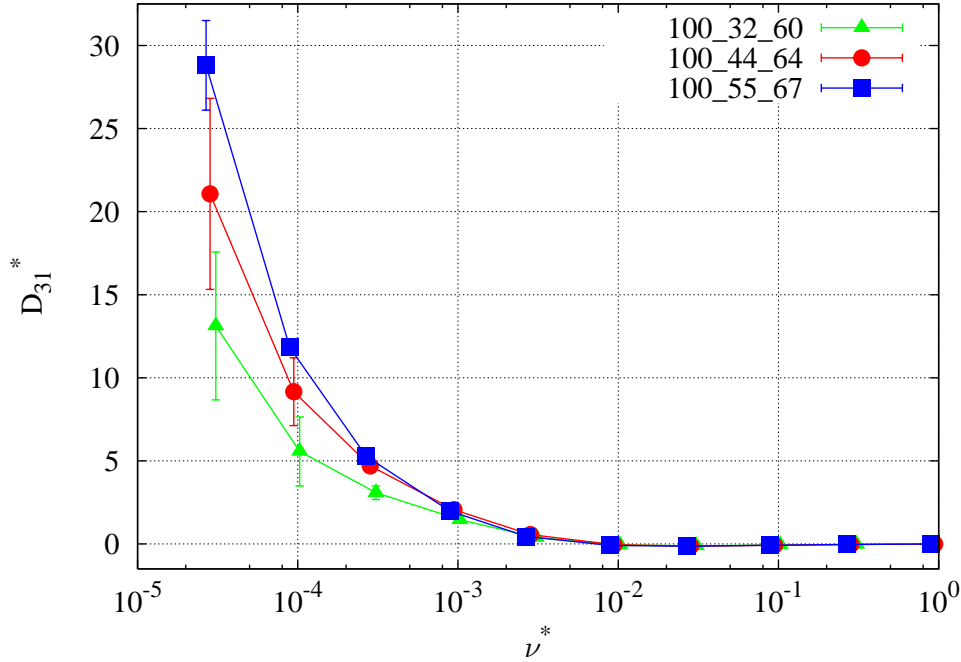


**Figure 13.** Bootstrap current coefficient at  $\rho = 0.7$  as a function of the collisionality.

Finally, the sidebands not shown in Fig. 11 might yield different radial diffusion coefficients for different configurations. Although this situation is not likely to happen, the ambipolar equation would yield different radial electric fields for given plasma profiles, and thus different bootstrap current profiles. This calculation is left for future works.

#### 4. Conclusions

Calculations of the bootstrap current for the TJ-II stellarator are presented. The  $\delta f$  code NEO-MC, together with DKES, has allowed for the first time for the precise computation of the neoclassical bootstrap transport coefficient in the long mean free path regime of the vacuum configuration of TJ-II. The low error bars have allowed for a precise convolution of the monoenergetic coefficients. Since the calculation has been repeated at several radial positions, we are able for the very first time to calculate the radial profile of the bootstrap current of several plasmas of TJ-II with sufficient accuracy for comparison with experimental results. A Monte Carlo method for error estimation allows us to confirm the significance of the results.

The current profile is well understood in terms of the plasma profiles. Since the electrons are within the  $l_{mf}$  and the plateau regime for all the plasmas considered, the gradient in the electron temperature provides the main contribution to the total current density.

The results show qualitative agreement with previous calculations and measurements at TJ-II; future work includes comparison with CXRS and Rogowski coils measurements for real TJ-II discharges.

We have calculated the bootstrap coefficient for several configurations usually operated at TJ-II. The results suggest that the dependence of the bootstrap current on the magnetic configuration should be small, specially for NBI plasmas. A more comprehensive study is left for a future work.

This calculation will allow to quantify more accurately finite-beta effects in the studies on the relation between confinement and magnetic configuration. Additionally, these results must be kept in mind when estimating the EBW current drive at TJ-II.

## 5. Acknowledgments

The authors are grateful to S.P. Hirshman and D. Spong for the DKES and VMEC codes, to J. Geiger for his help with the VMEC code and to J.A. Alonso and E. Solano for useful discussions. This work was carried out within the Associations EURATOM-CIEMAT, ÖAW-EURATOM and IPP-EURATOM. Part of the work was funded by the Spanish Ministerio de Ciencia e Innovación, Spain, under Project ENE2008-06082/FTN and by the Austrian Science Foundation, FWF, under contract number P16797-N08.

## References

- [1] Peeters A G 2000 *Plasma Physics and Controlled Fusion* **42** B231 URL <http://stacks.iop.org/0741-3335/42/i=12B/a=318>
- [2] Helander P and Sigmar D J 2002 *Collisional transport in magnetized plasmas* vol 87 (Cambridge University Press)
- [3] Turkin Y, Maaßberg H, Beidler C D, Geiger J and Marushchenko N B 2006 *Fusion Science and Technology* **50** 387–394 URL <http://www.new.ans.org/pubs/journals/fst/a1260>
- [4] Alejaldre C, Alonso J, Almoguera L, Ascasióbar E, Baciero A, Balbín R, Blaumoser M, Botija J, Brañas B, de la Cal E, Cappa A, Carrasco R, Castejón F, Cepero J R, Cremy C, Doncel J, Dulya C, Estrada T, Fernández A, Francés M, Fuentes C, García A, García-Cortés I, Guasp J, Herranz J, Hidalgo C, Jiménez J A, Kirpichev I, Krivenski V, Labrador I, Lapayese F, Likin K, Liniers M, López-Fraguas A, López-Sánchez A, de la Luna E, Martín R, Martínez A, Medrano M, Méndez P, McCarthy K, Medina F, van Milligen B, Ochando M, Pacios L, Pastor I, Pedrosa M A, de la Peña A, Portas A, Qin J, Rodríguez-Rodrigo L, Salas A, Sánchez E, Sánchez J, Tabarés F, Tafalla D, Tribaldos V, Vega J, Zurro B, Akulina D, Fedyanin O I, Grebenshchikov S, Kharchev N, Meshcheryakov A, Barth R, van Dijk G, van der Meiden H and Petrov S 1999 *Plasma Physics and Controlled Fusion* **41** A539 URL <http://stacks.iop.org/0741-3335/41/i=3A/a=047>
- [5] Alejaldre C, Alonso J, Almoguera L, Ascasióbar E, Baciero A, Balbín R, Blaumoser M, Botija J, Brañas B, de la Cal E, Cappa A, Carrasco R, Castejón F, Cepero J R, Cremy C, Delgado J M, Doncel J, Dulya C, Estrada T, Fernández A, Fuentes C, García A, García-Cortés I, Guasp J, Herranz J, Hidalgo C, Jiménez J A, Kirpichev I, Krivenski V, Labrador I, Lapayese F, Likin K, Liniers M, López-Fraguas A, López-Sánchez A, de la Luna E, Martín R, Martínez A, Martínez-Laso L, Medrano M, Méndez P, McCarthy K J, Medina F, van Milligen B, Ochando M, Pacios L, Pastor I, Pedrosa M A, de la Peña A, Portas A, Qin J, Rodríguez-Rodrigo L, Salas A, Sánchez E, Sánchez J, Tabarés F, Tafalla D, Tribaldos V, Vega J, Zurro B, Akulina D, Fedyanin O I, Grebenshchikov S, Kharchev N, Meshcheryakov A, Sarkisian K A, Barth R, van Dijk G and van der Meiden H 1999 *Plasma Physics and Controlled Fusion* **41** B109 URL <http://stacks.iop.org/0741-3335/41/i=12B/a=307>
- [6] Ascasióbar E, Alejaldre C, Alonso J, Almoguera L, Baciero A, Balbín R, Blanco E, Blaumoser M, Botija J, Brañas B, Cappa A, Carrasco R, Castejón F, Cepero J R, Chmyga A A, Doncel J, Dreval N B, Eguilior S, Eliseev L, Estrada T, Fedyanin O, Fernández A, Fontdecaba J M, Fuentes C, García A, García-Cortés I, Goncalves B, Guasp J, Herranz J, Hidalgo A, Hidalgo C,

- Jiménez J A, Kirpichev I, Khrebtov S M, Komarov A D, Kozachok A S, Krupnik L, Lapayese F, Likin K, Liniers M, López-Bruna D, López-Fraguas A, López-Rázola J, López-Sánchez A, de la Luna E, Malaquias A, Martín R, Medrano M, Melnikov A V, Méndez P, McCarthy K J, Medina F, van Milligen B, Nedzelskiy I S, Ochando M, Pacios L, Pastor I, Pedrosa M A, de la Peña A, Petrov A, Petrov S, Portas A, Romero J, Rodríguez-Rodrigo L, Salas A, Sánchez E, Sánchez J, Sarkisian K, Schchepetov S, Skvortsova N, Tabarés F, Tafalla D, Tribaldos V, Varandas C F A, Vega J and Zurro B 2002 *Plasma Physics and Controlled Fusion* **44** B307 URL <http://stacks.iop.org/0741-3335/44/i=12B/a=322>
- [7] Ascasíbar E, Estrada T, Castejón F, López-Fraguas A, Pastor I, Sánchez J, Stroth U, Qin J and the TJ-II Team 2005 *Nuclear Fusion* **45** 276 URL <http://stacks.iop.org/0029-5515/45/i=4/a=009>
- [8] Castellano J, Jimenez J A, Hidalgo C, Pedrosa M A, Fraguas A L, Pastor I, Herranz J, Alejaldre C and the TJ-II Team 2002 *Physics of Plasmas* **9** 713–716 URL <http://link.aip.org/link/?PHP/9/713/1>
- [9] López-Bruna D, Romero J A, Jiménez-Gómez R, Pedrosa M A, Ochando M, Estrada T, López-Fraguas A, Medina F, Herranz J, Kalhoff T, Ascasíbar E, de la Peña A, Lapayese F and Alonso J 2009 *Nuclear Fusion* **49** 085016 URL <http://stacks.iop.org/0029-5515/49/i=8/a=085016>
- [10] Castejón F, Fujisawa A, Ida K, Talmadge J N, Estrada T, López-Bruna D, Hidalgo C, Krupnik L and Melnikov A 2005 *Plasma Physics and Controlled Fusion* **47** B53 URL <http://stacks.iop.org/0741-3335/47/i=12B/a=S05>
- [11] Fernández A, Sarkisyan K, Matveev N, García A, Medrano M, Doane J, Moeller C, Doncel J, Pardo A, Cappa A, Castejón F, Khartchev N, Tereshchenko M, Tolkachev A and Catalán G 2005 *Fusion Engineering and Design* **74** 325 – 329 ISSN 0920-3796 Proceedings of the 23rd Symposium of Fusion Technology - SOFT 23 URL <http://www.sciencedirect.com/science/article/pii/S0920379605000384>
- [12] García-Regaña J M, Cappa A, Castejón F, Caughman J B O, Tereshchenko M, Ros A, Rasmussen D A and Wilgen J B 2011 *Plasma Physics and Controlled Fusion* **53** 065009 URL <http://stacks.iop.org/0741-3335/53/i=6/a=065009>
- [13] Castejón F, Velasco J L, García-Regaña J M, Allmaier K and Cappa A 2011 Electron Bernstein driven and bootstrap current estimations in the tj-ii stellarator *Proceedings of the 23rd IAEA Fusion Energy Conference, Daejeon* pp THW/P7–16
- [14] Hirshman S P, Shaing K C, van Rij W I, Beasley C O and Crume E C 1986 *Physics of Fluids* **29** 2951–2959 URL <http://link.aip.org/link/?PFL/29/2951/1>
- [15] Maaßberg H, Romé M, Erckmann V, Geiger J, Laqua H P, Marushchenko N B and the W7-AS Team 2005 *Plasma Physics and Controlled Fusion* **47** 1137 URL <http://stacks.iop.org/0741-3335/47/i=8/a=002>
- [16] Isaev M Y, Watanabe K Y, Cooper W A, Yokoyama M, Yamada H, Sauter O, Tran T M, Bergmann A, Beidler C and Maaßberg H 2009 *Nuclear Fusion* **49** 075013 URL <http://stacks.iop.org/0029-5515/49/i=7/a=075013>
- [17] Maaßberg H, Beidler C D and Turkin Y 2009 *Physics of Plasmas* **16** 072504 URL <http://link.aip.org/link/?PHP/16/072504/1>
- [18] Nishimura S, Motojima G, Nakamura Y, Okada H, Kobayashi S, Yamamoto S, Nagasaki K, Hanatani K, Kondo K *et al.* 2009 *Journal of Plasma and Fusion Research* **8** 1003 URL [http://www.jspf.or.jp/JPFRR/PDF/Vol8/jpfrs2009\\_08-1003.pdf](http://www.jspf.or.jp/JPFRR/PDF/Vol8/jpfrs2009_08-1003.pdf)
- [19] Beidler C D, Allmaier K, Isaev M Y, Kasilov S V, Kernbichler W, Leitold G O, Maaßberg H, Mikkelsen D R, urakami S M, Schmidt M, Spong D A, Tribaldos V and Wakasa A 2011 *Nuclear Fusion* **51** 076001 URL <http://stacks.iop.org/0029-5515/51/i=7/a=076001>
- [20] Ribeiro E R S and Shaing K C 1987 *Physics of Fluids* **30** 462–466 URL <http://link.aip.org/link/?PFL/30/462/1>
- [21] Rodríguez Yunta A v R V I and P H S 1990 Bootstrap currents in heliac tj-ii configurations *Proceedings of the 17th European Conference on Controlled Fusion and Plasma Heating, Amsterdam* vol 14B p 505
- [22] Tribaldos V Maaßberg H J J A and Varias A 2003 Bootstrap current simulations for the tj-ii stellarator *Proceedings of the 30th EPS Conference on Controlled Fusion and Plasma Physics, St. Petersburg* vol 27A p P1.28 URL [http://crppc42.epfl.ch/StPetersburg/PDFS/P1\\_028.pdf](http://crppc42.epfl.ch/StPetersburg/PDFS/P1_028.pdf)
- [23] Allmaier K, Kasilov S V, Kernbichler W and Leitold G O 2008 *Physics of Plasmas* **15** 072512 URL <http://link.aip.org/link/?PHP/15/072512/1>
- [24] Sugama H and Nishimura S 2002 *Physics of Plasmas* **9** 4637–4653 URL <http://link.aip.org/link/?PHP/9/4637/1>
- [25] Beidler C D, Isaev M Y, Kasilov S V, Kernbichler W, Murakami H M S, Nemov V V, Spong D and Tribaldos V 2007 Icns-impact of incompressible

- ex b flow in estimating mono-energetic transport coefficients *Proceedings of the 16th Int. Stellarator/Heliotron Workshop, Toki* vol NIFS-PROC-69 p P2.O31 URL [http://www.nifs.ac.jp/itc/itc17/file/PDF\\_proceedings/poster2/P2-031.pdf](http://www.nifs.ac.jp/itc/itc17/file/PDF_proceedings/poster2/P2-031.pdf)
- [26] Tribaldos V and Guasp J 2005 *Plasma Physics and Controlled Fusion* **47** 545 URL <http://stacks.iop.org/0741-3335/47/i=3/a=010>
- [27] Velasco J L, Castejon F and Tarancon A 2009 *Physics of Plasmas* **16** 052303 URL <http://link.aip.org/link/?PHP/16/052303/1>
- [28] Lotz W and Nuhrenberg J 1988 *Physics of Fluids* **31** 2984–2991 URL <http://link.aip.org/link/?PFL/31/2984/1>
- [29] Turkin Y, Beidler C D, Maaßberg H, Murakami S, Tribaldos V and Wakasa A 2011 *Physics of Plasmas* **18** 022505 URL <http://link.aip.org/link/?PHP/18/022505/1>
- [30] Shaing K C and Callen J D 1983 *Physics of Fluids* **26** 3315–3326 URL <http://link.aip.org/link/?PFL/26/3315/1>
- [31] Nakajima N, Okamoto M, Todoroki J, Nakamura Y and Wakatani M 1989 *Nuclear Fusion* **29** 605 URL <http://stacks.iop.org/0029-5515/29/i=4/a=006>
- [32] Kernbichler W, Kasilov S V, Nemov V V, Leitold G O and Heyn M F 2002 Evaluation of the bootstrap current in stellarators *Proceedings of the 29th EPS Conference on Plasma Physics and Controlled Fusion, Montreux* vol 26B p P2.100 URL [https://crppwww.epfl.ch/~duval/p2\\_100.pdf](https://crppwww.epfl.ch/~duval/p2_100.pdf)
- [33] Spong D A 2005 *Physics of Plasmas* **12** 056114 URL <http://link.aip.org/link/?PHP/12/056114/1>
- [34] Estrada T, de la Luna E, Ascasibar E, Jiménez J A, Castejón F, García-Cortés I, López-Fraguas A, Sánchez J and Tribaldos V 2002 *Plasma Physics and Controlled Fusion* **44** 1615 URL <http://stacks.iop.org/0741-3335/44/i=8/a=313>
- [35] Rapisarda D, Zurro B, Baciero A, Tribaldos V, Ascasibar E *et al.* 2005 An investigation of the relationship between toroidal rotation and bootstrap current in the tj-ii stellarator *Europhysics Conference Abstracts: 32nd Conf. Plasma Physics, Tarragona* vol 29C p P2.086 URL [http://eps2005.ciemat.es/papers/pdf2/P2\\_086.pdf](http://eps2005.ciemat.es/papers/pdf2/P2_086.pdf)
- [36] Sánchez J, Acedo M, Alonso A, Alonso J, Alvarez P, Ascasibar E, Baciero A, Balbín R, Barrera L, Blanco E, Botija J, de Bustos A, de la Cal E, Calvo I, Cappa A, Carmona J M, Carralero D, Carrasco R, Carreras B A, Castejón F, Castro R, Catalán G, Chmyga A, Chamorro M, Eliseev L, Esteban L, Estrada T, Fernández A, Fernández-Gavilán R, Ferreira J A, Fontdecaba J M, Fuentes C, García L, García-Cortés I, García-Gómez R, García-Regaña J M, Guasp J, Guimaraes L, Happel T, Hernanz J, Herranz J, Hidalgo C, Jiménez J A, Jiménez-Denche A, Jiménez-Gómez R, Jiménez-Rey D, Kirpichev I, Komarov A D, Kozachok A S, Krupnik L, Lapayese F, Liniers M, López-Bruna D, López-Fraguas A, López-Rázola J, López-Sánchez A, Lysenko S, Marcon G, Martín F, Maurin V, McCarthy K J, Medina F, Medrano M, Melnikov A V, Méndez P, van Milligen B, Mirones E, Nedzelskiy I S, Ochando M, Olivares J, de Pablos J L, Pacios L, Pastor I, Pedrosa M A, de la Peña A, Pereira A, Pérez G, Pérez-Risco D, Petrov A, Petrov S, Portas A, Pretty D, Rapisarda D, Rattá G, Reynolds J M, Rincón E, Ríos L, Rodríguez C, Romero J A, Ros A, Salas A, Sánchez M, Sánchez E, Sánchez-Sarabia E, Sarkisian K, Sebastián J A, Silva C, Schchepetov S, Skvortsova N, Solano E R, Soletto A, Tabarés F, Tafalla D, Tarancón A, Tashev Y, Tera J, Tolkachev A, Tribaldos V, Vargas V I, Vega J, Velasco G, Velasco J L, Weber M, Wolfers G and Zurro B 2009 *Nuclear Fusion* **49** 104018 URL <http://stacks.iop.org/0029-5515/49/i=10/a=104018>
- [37] Mynick H E and Hitchon W N G 1983 *Nuclear Fusion* **23** 1053 URL <http://stacks.iop.org/0029-5515/23/i=8/a=006>
- [38] Hirshman S P, van Rij W I and Merkel P 1986 *Computer Physics Communications* **43** 143 – 155 ISSN 0010-4655 URL <http://www.sciencedirect.com/science/article/pii/0010465586900585>
- [39] Watanabe K, Nakajima N, Okamoto M, Nakamura Y and Wakatani M 1992 *Nuclear Fusion* **32** 1499 URL <http://stacks.iop.org/0029-5515/32/i=9/a=I01>
- [40] i Margalet S F, Cooper W A, Allfrey S J, Popovitch P and Isaev M Y 2004 *Fusion Science and Technology* **46** 44 URL <http://epubs.ans.org/?a=539>
- [41] Solano E R, Rome J A and Hirshman S P 1988 *Nuclear Fusion* **28** 157 URL <http://stacks.iop.org/0029-5515/28/i=1/a=013>